J Mater Sci (2011) 46:2741–2747
DOI 10.1007/s10853-010-5147-3

The compressive response of a titanium foam at low and high strain rates

P. Siegkas · V. L. Tagarielli · N. Petrinic · L. P. Lefebvre

Received: 22 September 2010 / Accepted: 30 November 2010 / Published online: 16 December 2010

Abstract Sintered titanium powder and titanium foams of relative density ranging from 0.3 to 0.9 were produced by powder metallurgy routes and tested in uniaxial compression at low, medium and high rates of strain. At all strain rates, the foams deform by plastic collapse of the pores, accompanied by micro-cracking at compressive strains exceeding 0.2. The foams investigated are strain rate sensitive, with both the yield stress and the strain hardening rate increasing with applied strain rate. The strain rate sensitivity is more pronounced for foams of lower relative density.

Introduction

Titanium and Ti alloys possess widespread application in engineering construction due to their high specific stiffness and strength, combined with good high temperature mechanical performance, corrosion resistance, biocompatibility; Ti and its alloys can also be characterized by pronounced strain hardening [1] and possess good impact resistance due to their strain rate sensitivity [2].

Powder sintering routes allow production of cellular solids [3] made from Ti and Ti alloys [4, 5]. These materials are of interest to the aerospace and defence industry due to their good dynamic specific energy absorption, and attract the attention of the bio-medical industry due to good mechanical properties combined with biocompatibility.

While the static and dynamic mechanical response of Ti and Ti alloys have been investigated by many authors (see for example [6–8]), less work exists on the response of Ti and Ti alloy foams. Several authors conducted quasi-static compression, tension and bending tests experiments on open-cell [9, 10] and closed-cell [11] Ti foams manufactured by the space-holder method, which consists in compacting and sintering a mixture of Ti powder and a polymeric space-holder in order to obtain pores of controllable size. Experiments revealed that the foams can be anisotropic as a consequence of the compaction process, and that the mechanical properties of these foams were similar to those of cancellous and cortical bone, for the lower and higher relative densities, respectively.

Tuncer and Arslan [12] tested in compression Ti foams of relative density $\bar{\rho} = 0.3 - 0.8$, produced by optimizing the space-holder method. The materials were deformed at low and medium strain rates (10^{-3}–6×10^{2} s^{-1}) and the foams were found to be mildly strain rate sensitive in this range. Thelen et al. [13] worked with sintered foams obtained from both commercially pure Ti and $TiAl_6V_4$ powders. Compressed argon gas was used as a foaming agent to obtain relative densities in the range $\bar{\rho} = 0.2 - 0.5$. Specimens were subjected to quasi-static mechanical loading in order to determine their elastic properties and the variation of these with the foam relative density. It was found that several analytical models (e.g., Mori and Tanaka [14], Ashby and Gibson [15]) were able to predict accurately the foam stiffness.

The fragmented existing experimental studies suggest that Ti foams can be mildly sensitive to strain rate when loaded in compression. This is in contrast with the results reported by other authors on different metallic foams, see

P. Siegkas · V. L. Tagarielli (✉) · N. Petrinic
Department of Engineering Science, Universiy of Oxford, Parks Road, Oxford OX1 3PJ, UK
e-mail: vito.tagarielli@eng.ox.ac.uk

L. P. Lefebvre
National Research Council Canada, Industrial Materials Institute, 75 de Mortagne, Boucherville, QC J4B 6Y4, Canada

for example Deshpande and Fleck [16, 17] on aluminium foams; these authors tested aluminium foams of low relative density ($\bar{\rho} \approx 0.1$) and found that the compressive response was strain rate insensitive.

In this study, we focus on the compressive properties of pure Ti foams produced using a powder metallurgy process [18], and the measured responses are compared with those of Ti powder sintered under similar conditions to the foams. In order to understand the dependence of the material response on the relative density and the imposed strain rate, foams with relative density in the range $\bar{\rho} = 0.35 - 0.55$ are tested in compression at strain rates ranging from 10^{-2} to 2×10^{3} s^{-1}, and results are compared with those obtained for sintered Ti powders of relative density 0.9.

Material and experiments

Material manufacturing

Sintered Ti powders and sintered Ti foams were produced using the process described in [18]. Briefly, titanium powder is mixed with a binder and a chemical foaming agent. The resulting mixture is poured into a mold and heated in order to foster the foaming process; subsequently, the material is de-binded and sintered.

During foaming the binder melts and forms a suspension with the Ti particles. The foaming agent then decomposes and generates a gas that expands the suspensions; after foaming, the binder is eliminated by thermal decomposition. Specimens with different porosity levels are produced by modifying the composition of the mixture. The resulting material is cut into circular cylindrical specimens which are then sintered at high temperature to consolidate the material. Sintered Ti powder specimens were produced by a similar route to that described above, absent the foaming agent and the binder.

SEM analysis of the material microstructure

Scanning electron microscopy (SEM) was used to examine the microstructure of the sintered Ti foams. Two levels of porosity are clearly visible in the foam: (i) a macro-porosity which results from the foaming process and (ii) a micro-porosity resulting from incomplete consolidation of the Ti powder during sintering, as shown in Fig. 1.

The microstructure of the sintered powders ($\bar{\rho} = 0.9$) comprised well sintered particles and only small micro-pores of diameter around 10 μm were observed. On the other hand, all foams ($\bar{\rho} = 0.35 - 0.55$) displayed macroscopic pores of diameter ranging from 100 to 1400 μm. The micro-porosity was also higher in the foams, due to the effect of the binder and foaming agent on the inter-particle spacing after sintering.

X-ray tomography analysis

In order to observe the foams microstructure, X-ray tomography analysis was performed on circular cylinders (5 mm diameter and height) of different relative densities, ranging from 0.35 to 0.55. A SkyScan (Kartuizersweg 3B, 2550 Kontich, Belgium) X-ray tomographer of spatial resolution of 9 μm was used to produce two-dimensional cross-section images of the foam microstructure, which allowed automated reconstruction of the three-dimensional foam structure.

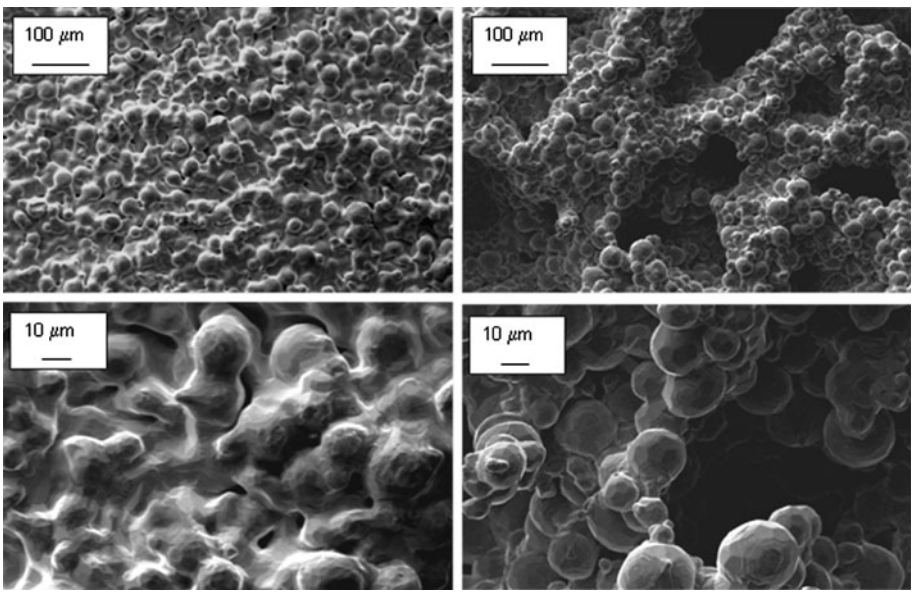

Fig. 1 SEM images of high-relative density ($\bar{\rho} = 0.91$, *left*) and low-density ($\bar{\rho} = 0.45$, *right*) materials at two different magnifications. Micro-pores of diameter around 10 μm are seen in the sintered powder (high-density material); larger macro-pores of diameter on the order of 100 μm are observed in the low-density foam. Consolidation (i.e., degree of sintering) is higher for the sintered powder

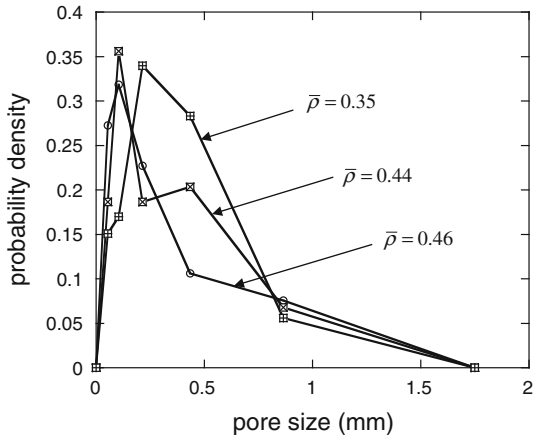

Fig. 2 Pore size distributions for Ti foams of three different densities. The peak of the distribution occurs at smaller pore diameters as the density increases

For all foam densities, the microstructure comprised a network of sintered particles surrounding a random distribution of pores of irregular shape, with no preferential orientation. The X-ray tomographer software (Skyscan CTan) methods were employed to measure the pore size distribution in each sample, as presented in Fig. 2 for three different foam densities. The entire volume of the foam samples (100 mm^2) was analyzed, corresponding to a number of pores in excess of 1000. Pore diameters were calculated as the diameter of spheres of volume equivalent to the volume of the pores. Foams of higher density are associated with a smaller average pore size, as shown by the different peaks in the three measured pore size distributions.

Quasi-static uniaxial compression

Porous specimens of density $\bar{\rho} = 0.35 - 0.93$ were tested in uniaxial compression at a strain rate of 10^{-2} s^{-1}. Preliminary compression experiments revealed that the material response was approximately isotropic. Then, circular cylindrical specimens of diameter 11 mm and height of 13 mm were compressed in the axial direction. A screw driven machine in displacement control was used to conduct the experiments. The compressive force was measured by a resistive load cell, and the shortening of the sample was measured by a laser extensometer and was used to calculate the compressive strain. Experiments were interrupted when an axial strain larger than 0.5 was achieved.

An optical system was used to monitor deformation of the sample. Figure 3 shows photographs taken during a quasi-static compression test, at different levels of imposed axial strain. The figure shows that the plastic deformation of the foam is initially uniform, with negligible barrelling. At axial strains larger than 0.2, barrelling of the sample is observed in conjunction with formation of small cracks. These cracks coalesce at high compressive strains to give catastrophic failure of the sample.

Figure 4 represents the measured stress versus strain curves for samples of four different densities. For all densities, the material response comprises an initial linear phase followed by a strain hardening response. The elastic

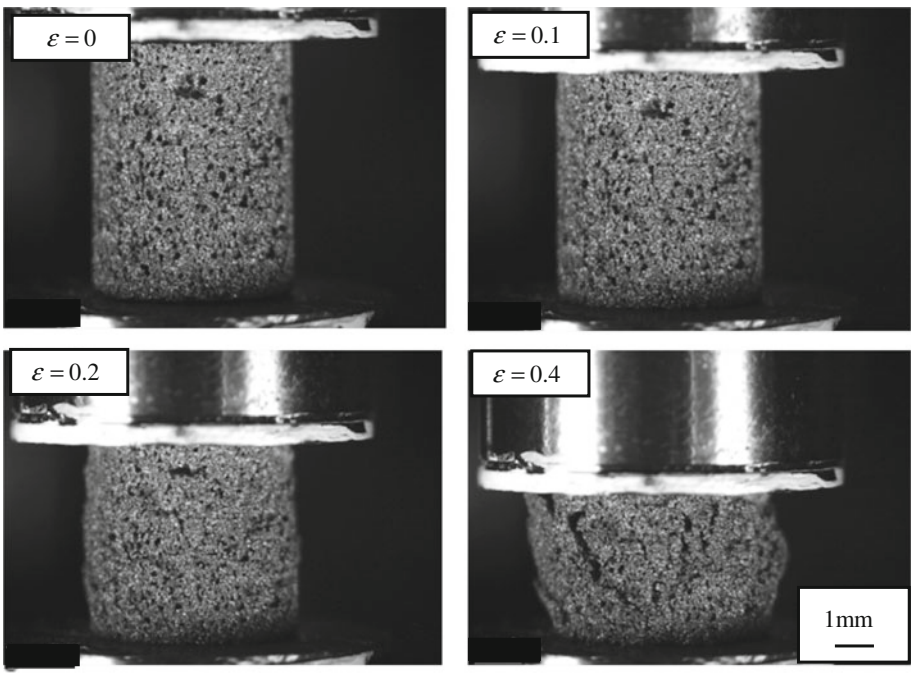

Fig. 3 Photographs of a foam specimen of density $\bar{\rho} = 0.37$ subject to a quasi-static compression experiment. Deformation is initially uniform; micro-cracking intervenes at axial strains higher than 0.2

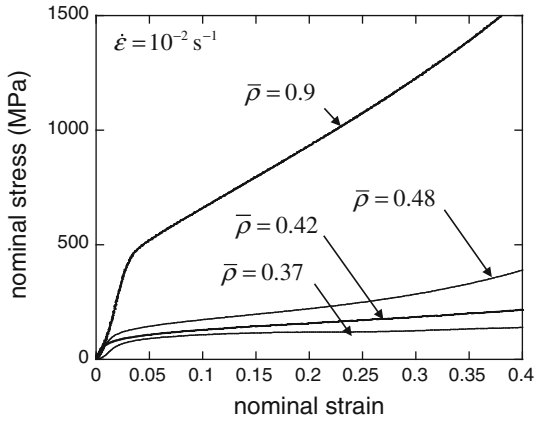

Fig. 4 Quasi-static compressive response of the Ti foams and sintered Ti powder

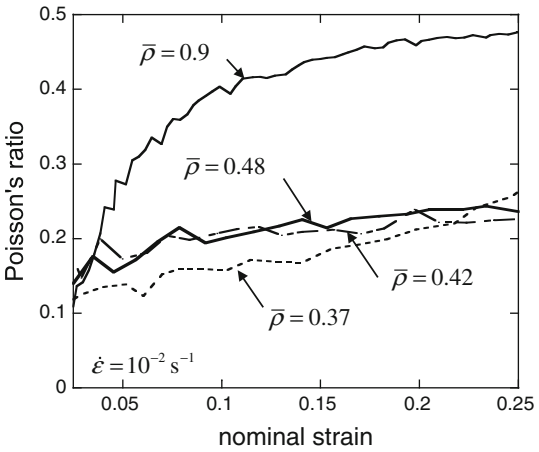

Fig. 5 Measured Poisson's ratio as a function of the applied axial strain, for foams of four different densities

modulus of the material was measured using unloading and reloading at a plastic compressive strain of 0.1, and the modulus was found to increase with increasing density. The material yield stress was recorded for each test; this was defined as the flow stress at a nominal compressive plastic strain of 0.2. The strain hardening rate was higher for foams of higher density. Selected compression tests were also repeated on specimens of different dimensions (11 mm diameter and 5 mm height). The measured response was found to be independent of the specimen height.

An in-house developed image correlation software was used to measure transverse deformation of the sample; the ratio of this transverse strain to the imposed compressive axial strain is defined here as the material Poisson's ratio. Figure 5 shows the evolution of this ratio with increasing imposed axial strain, for a range of foam densities. This data are shown for axial strains less than 0.25. Beyond this

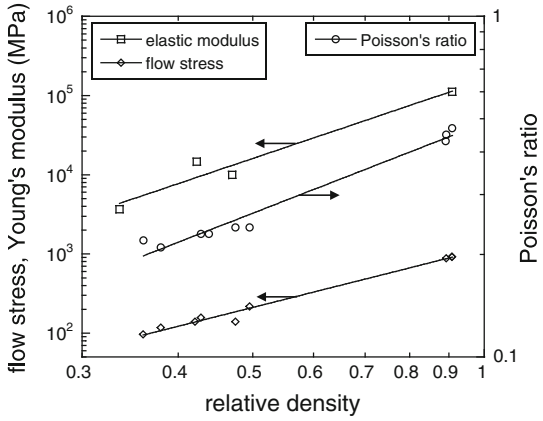

Fig. 6 Variation of elastic modulus, flow stress (at 0.2 axial plastic strain) and Poisson's ratio (at 0.2 axial plastic strain) as a function of relative density. The graph includes power-law fits of the experimental data

value of imposed strain, material cracking intervened in the experiments, invalidating Poisson's ratio measurements.

The initial value of the Poisson ratio (corresponding to elastic axial strains) is in the range 0.1–0.15 for all foam densities; these values are a little bit lower than those measured by other authors [19] by laser ultrasonic probing on foams produced under slightly different processing conditions. As the axial strain increases, the Poisson's ratio also increases at a rate depending on the foam density. For the foams tested, the Poisson's ratio shows a mild increase with strain, attaining a value of 0.2 when the axial strain reaches 0.2; in contrast, for the sintered powders, the increase of Poisson's ratio with axial strain is more pronounced and tends to approach the theoretical limit of 0.5 (for a plastically incompressible material) at large imposed axial strains.

Figure 6 represents the dependence of compressive elastic modulus, yield stress and Poisson's ratio (at an axial strain of 0.2) on the foam relative density; experimental data are accompanied by least-square power-law fits. The exponent of the power laws describing the dependence of Young's modulus and yield stress on relative density are 3.28 and 2.44, respectively (Ashby and Gibson [15] predict coefficients of 2 and 1.5, respectively, for low-density open-cell foams).

In situ SEM compression experiments

With the aim of visualizing the microscopic compressive deformation and failure mechanisms for the foams under investigation, cubic specimens of 5 mm side were cut from foams of relative density $\bar{\rho} = 0.35 - 0.44$ and loaded in compression in a SEM. A 5 kN miniature loading rig was used to compress the specimens at a strain rate of $10^{-2}\ s^{-1}$; the tests were periodically interrupted to allow a scan to be

taken. The sequence of SEM micrographs produced, not reported here for the sake of brevity, allowed to visualize deformation and failure mechanisms of the foam in uniaxial compression.

It was observed that macro-pores (of diameter on the order of 100 μm) progressively collapsed by flattening along planes perpendicular to the loading direction. At compressive strains exceeding 0.2, micro-cracking was observed, with cracks of length of the order of 50 μm initiating and propagating. Propagation of these micro-cracks occurred both at the sintering necks between powder particles and across the powder particles. The observed deformation mechanisms were independent of foam relative density in the range investigated.

Dynamic compression experiments

In order to measure the dependence of the material response upon the rate of strain, dynamic uniaxial compression tests were performed on cylindrical specimens of diameter 11 mm and height 5 mm. Two different loading systems were employed to obtain strain rates of the order of 10 s^{-1} (medium) and 2 × 10^3 s^{-1} (high), respectively, as detailed below.

Medium rate experiments

A hydraulic loading machine was used to load the sample. A light steel piston compressed the foam specimens by moving at velocities of the order of 0.05 ms^{-1}, corresponding to an imposed strain rates of the order of 10 s^{-1}. The maximum achievable axial strain was limited to a maximum of 0.3 by the capacity of the loading system. High-speed photography was employed to observe the experiments during deformation. The load was measured by a resistive load cell while the shortening of the sample was measured by both LVDT transducers as well as by optical methods. The material response (see Figs. 7; 8) was similar to that observed in quasi-static tests, comprising an elastic phase followed by a strain hardening regime. For all materials, the measured yield stress was significantly larger at this strain rate than that measured in the quasi-static tests.

High rate experiments

In order to achieve a strain rate of 2 × 10^3 s^{-1}, a split pressure Hopkinson bar (SPHB) setup was used [20], with all bars made from hardened steel. The forces acting on the specimen ends were recorded by the strain gauges on the input and output bars, and the sample shortening was estimated via both stress wave analysis and high-speed photography. Force equilibrium was typically reached after 10 μs, corresponding to an axial strain around 0.03, and the imposed strain rate was approximately constant after this time.

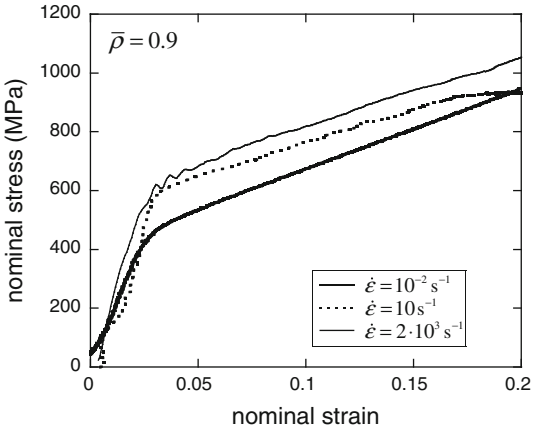

Fig. 7 Compressive nominal stress versus strain response of sintered powder of relative density $\bar{\rho} = 0.9$ at low, medium and high strain rates

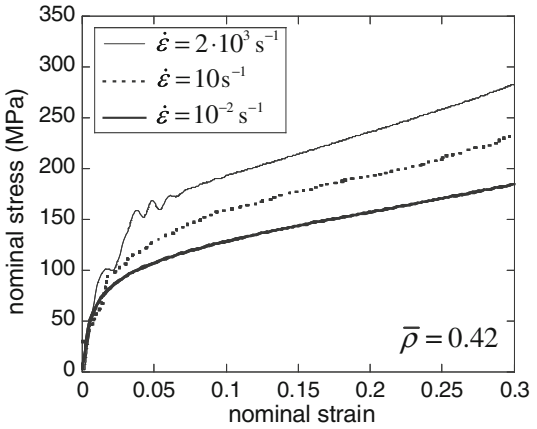

Fig. 8 Compressive nominal stress versus strain response of a foam of relative density $\bar{\rho} = 0.42$ at low, medium and high strain rates

Figure 7 represents a comparison of the stress versus strain response of the sintered powder ($\bar{\rho} = 0.9$) at different strain rates. Recall that the microstructure of this material was associated with pores of diameter of the order of 10 μm. The initial apparent stiffness was independent of strain rate, whereas the yield stress increased by approximately 33% as the strain rate increased from 10^{-3} to 10^3 s^{-1}. The strain hardening rate was insensitive to imposed strain rate.

Figure 8 shows a similar comparison of the stress versus strain responses for a foam of density $\bar{\rho} = 0.42$, which was shown to contain pores of diameter of the order of 100 μm. While the material stiffness seems independent of the strain rate, the yield stress increases with increasing strain rates. In contrast with what was observed for the sintered powder,

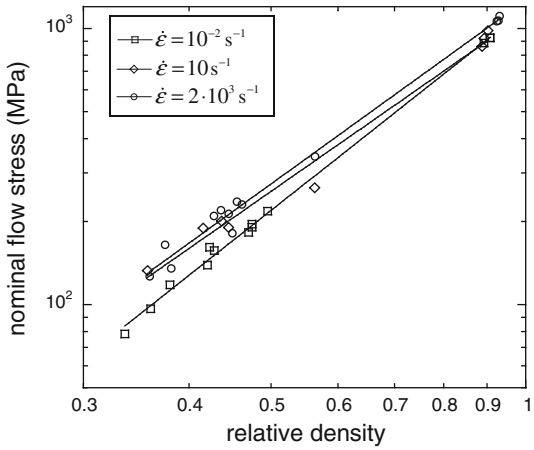

Fig. 9 Measured flow stress (at a plastic strain of 0.2) as a function of foam density, in low, medium and high strain rate experiments

the strain hardening rate also displayed a mild increase with increasing strain rate.

Both quasi-static and dynamic experiments were repeated at least three times for each strain rate and each foam density considered, in order to measure the scatter of the results; this scatter was significant, due to the small size of the specimens and to the highly irregular microstructure.

The variation of the yield stress as a function of density and strain rate is presented in Fig. 9. At each strain rate, the yield stress varies with foam density according to a power-law with exponent and intercept depending on the imposed strain rate. It can be deduced from Fig. 9 that for low-density foams the yield stress increases by about 30% as the strain rate is increased from 10^{-3} to 2×10^3 s^{-1}. For sintered powders, the material strain rate sensitivity seems to be lower: the yield stress increases by only 13% with the same increase in strain rate.

Concluding discussion

Porous solids made from sintered commercially pure Ti powder were studied; the microstructure of these solids comprised (i) micro-pores (diameter 10 μm) of round, smooth shape, resulting from the incomplete sintering of the gaps between titanium powder particles and (ii) macro-pores (diameter > 100 μm) of irregular shape and sharp corners, formed by the decomposition of the foaming agent. The sintered Ti powder tested presented only micro-porosity, while the sintered Ti foams presented both micro- and macro-porosity.

Upon loading in compression foams initially deform elastically and subsequently collapse plastically by flattening of the macro-pores perpendicularly to the loading direction. For the sintered powder ($\bar{\rho} = 0.9$), produced without binder and foaming agent, plastic collapse occurs by flattening of the micro-pores. The pore-flattening mechanism is accompanied by transverse strain; the Poisson's ratio is found to increase with the imposed axial strain at a rate depending on the foam density. At compressive axial strains in the range 0.15–0.3, micro-cracking is observed. At sufficiently high axial strains the strain hardening rate increases for these foams, due to material densification by complete closure of the pores. The densification strain increases as the foam relative density decreases.

The mechanical response of the foams is sensitive to relative density; elastic modulus, yield stress and the strain hardening rate increase with the foam relative density. Comparisons of the measured stress–strain responses at different strain rates revealed that the material response is sensitive to the applied strain rate.

Sintered Ti powder ($\bar{\rho} = 0.9$) displays an increase of the yield stress with strain rate comparable to those observed by other authors [6–8] for fully dense crystalline Ti alloys. This elevation in yield stress was measured to be of 13% as the strain rate was varied from 10^{-2} to 2×10^3 s^{-1}; for these sintered powders, the strain hardening rate is independent of the applied strain rates.

Foams ($\bar{\rho} = 0.3 - 0.5$) display an elevation of both yield stress and strain hardening rate with increasing applied strain rate. The strain rate sensitivity appears to be more pronounced for foams of lower relative density: foams with relative density $\bar{\rho} = 0.33$ displayed an elevation of 32% in flow stress (at a plastic strain of 0.2) as the strain rate was varied from 10^{-2} to 2×10^3 s^{-1}. Deformation mechanisms observed via quasi-static in situ testing for the foams were insensitive to relative density, and it may be conjectured that the presence of large pores in the foams microstructure results in micro-inertial stress fields, affecting the measured macroscopic flow stress. However, this is not the only possible explanation for the enhanced strain rate sensitivity in foams compared to that observed in sintered Ti powders: in case of high strain rate loading, deformation and fracture mechanisms may depend on the level of porosity: microscopic observations of the dynamic foam deformation and fracture should be conducted in order to aid interpretation of the observed strain rate sensitivity.

Acknowledgements The authors acknowledge financial support of Rolls-Royce plc (Dr. J. Reed, maintenance for Mr. Siekgas) and National Research Council Canada (Industrial Materials Institute, material manufacturing). Vito Tagarielli is grateful to Mr. S. Carter and Mr. N. Warland for assistance with experiments and specimen preparation.

References

1. Long M, Rack HJ (1998) Biomaterials 19:1621
2. Nemat-Nasser S, Guo WG, Cheng JY (1999) Acta Mater 47(13):3705

3. Ashby MF, Evans AG, Fleck NA, Hutchinson JW, Wadley HNG, Gibson LJ (2000) Metal foams: a design guide.Butterworth-Heinemann. ISBN 0-7506-7219-6
4. Lefebvre L-P, Baril E, Bureau MN (2009) J Mater Sci Mater Med 20(11):2223
5. Jorgensen DJ, Dunand DC (2010) Mater Sci Eng A 527(3):849
6. Gudena M, Celikc E, Akara E, Cetiner S (2005) J Mater Charact 54(4–5):399
7. Rouxel A, Chiem CY (1988) Impact Load Dyn Behav Mater 2:601
8. Kruger L, Meyer LW, Razorenov SV, Kanel GI (2003) Int J Impact Eng 28(8):877
9. Wen CE, Yamada Y, Shimojima K, Chino Y, Asahina T, Mabuchi M (2002) J Mater Sci Mater Med 13:397
10. Wen CE, Mabuchi M, Yamada Y, Shimojima K, Chino Y, Asahina T (2001) Scr Mater 45(10):1147
11. Imwinkelried T (2006) J Biomed Mater Sci 81A(4):964
12. Tuncer N, Arslan G (2009) J Mater Sci 44:1477. doi: 10.1007/s10853-008-3167-z
13. Thelen S, Barthelat F, Brinson LC (2003) J Biomed Mater Sci 69A:601
14. Mori T, Tanaka K (1973) Acta Metall 21:571
15. Ashby MF, Gibson LJ (1997) Cellular solids: structure and properties. Cambridge University Press, New York
16. Deshpande VS, Fleck NA (2000) Int J Impact Eng 24:277
17. Radford DD, Deshpande VS, Fleck NA (2005) Int J Impact Eng 31(9):1152
18. Lefebvre L-P, Thomas Y (2003) US Patent No. 6,660,224 B2, 9 Dec 2003
19. Lefebvre LP, Blouin A, Rochon SM, Bureau MN (2006) Adv Eng Mater 8(9):841
20. Gray GT (2000) ASM Int 8:462